Publication Year	2020
Acceptance in OA	2021-11-23T10:08:33Z
Title	Orbital and spectral characterization of the benchmark T-type brown dwarf HD 19467B
Authors	Maire, A. -L., Molaverdikhani, K., Desidera, S., Trifonov, T., Mollière, P., D'ORAZI, VALENTINA, Frankel, N., Baudino, J. -L., MESSINA, Sergio, Müller, A., Charnay, B., Cheetham, A. C., Delorme, P., LIGI, ROXANNE, Bonnefoy, M., Brandner, W., MESA, DINO, Cantalloube, F., Galicher, R., Henning, T., Biller, B. A., Hagelberg, J., Lagrange, A. -M., Lavie, B., Rickman, E., Ségransan, D., Udry, S., Chauvin, G., GRATTON, Raffaele, Langlois, M., Vigan, A., Meyer, M. R., Beuzit, J. -L., Bhowmik, T., Boccaletti, A., Lazzoni, C., Perrot, C., Schmidt, T., Zurlo, A., Gluck, L., Pragt, J., Ramos, J., Roelfsema, R., Roux, A., Sauvage, J. -F.
Publisher's version (DOI)	10.1051/0004-6361/202037984
Handle	http://hdl.handle.net/20.500.12386/31119
Journal	ASTRONOMY & ASTROPHYSICS
Volume	639

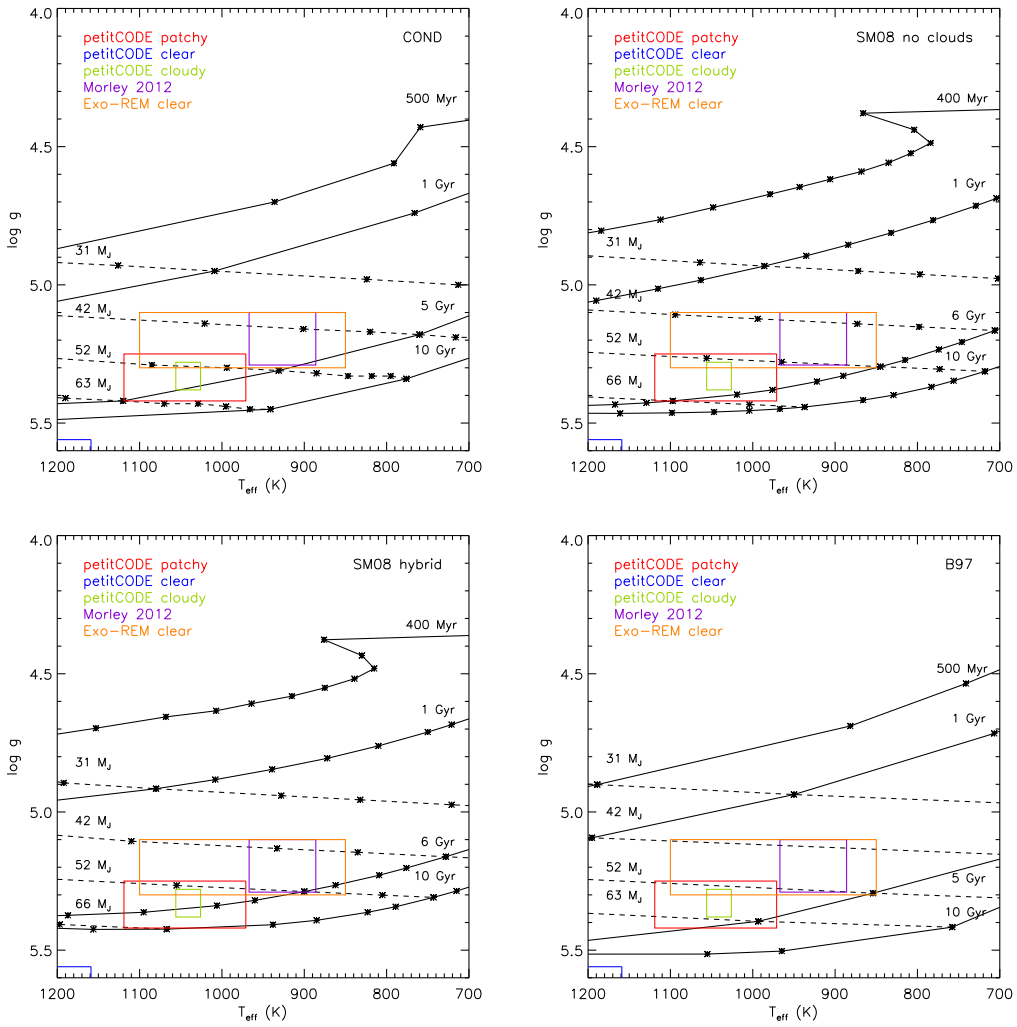

Fig. 17. Surface gravity as a function of the effective temperature predicted for several ages (black solid curves) and companion masses (dashed curves) by the models COND, the models of Saumon & Marley (2008) for two treatments of the clouds, and the models of Burrows et al. (1997). For comparison, the parameters derived from the atmospheric fits are shown (colored rectangles, Sect. 5.2).

Figure 16 shows the estimated bolometric luminosity (from the K_s-band magnitude), effective temperature, and age of HD 19467B with the predictions from the models COND (Baraffe et al. 2003), of Saumon & Marley (2008) (for two treatments of the clouds, hybrid and no clouds), and of Burrows et al. (1997) assuming for the companion mass 74^{+3}_{-9} M_J (Sect. 4.4). The hybrid cloudy model of Saumon & Marley (2008) intends to model the disappearance of the clouds at the L/T transition by increasing the cloud sedimentation parameter with decreasing $T_{\rm eff}$. The evolution model was computed assuming for the atmosphere model a combination of cloudless and cloudy atmosphere models. We consider for the effective temperature the constraints from the petitCODE fit with patchy clouds (Sect. 5.2). We could not test the recent models of Baraffe et al. (2015) because they do not extend to effective temperatures below ~1600 K for the age range of HD 19467B. The measured bolometric luminosity, age, and dynamical mass of the companion are better reproduced by the models of Burrows et al. (1997). The other models tend to overestimate its luminosity or equivalently to underestimate its cooling. When considering the effective temperature instead of the bolometric luminosity, the properties of the companion are compatible with more models, but are better reproduced by the models of Burrows et al. (1997) and the cloudless models of Saumon & Marley (2008).

Dieterich et al. (2018) find that evolutionary models tend to underpredict the cooling rate of ϵ Ind C and that evolutionary models employing model atmospheres with lower molecular opacities reproduce its measured mass better. Brandt et al. (2019a) find that when assuming an age older than 5 Gyr the models of Burrows et al. (1997) reproduce the measured mass of GJ 229B better. Brandt et al. (2019b) find for GJ 758B that the models COND, the models of Burrows et al. (1997), and the models of Saumon & Marley (2008) without clouds and a hybrid cloud model are compatible with its measured mass for an age older than 6 Gyr.

Saumon & Marley (2008) discuss the differences between their models and the models COND and of Burrows et al. (1997). Briefly, the main differences between the cloudless models of Saumon & Marley (2008) and COND relevant to the case of an old and massive brown dwarf such as HD 19467B reside in the surface boundary condition provided by the atmosphere and the noninclusion in the former model of the electron conduction in the core of the object (which is a dominant energy transport mechanism). The noninclusion of the latter effect produces lower luminosities. For a 10-Gyr brown dwarf of 0.06 $M_\odot$, Saumon & Marley (2008) find a difference in bolometric luminosity of ~0.1 dex compared to the COND model. This value agrees with the luminosity shift found by Chabrier et al. (2000)

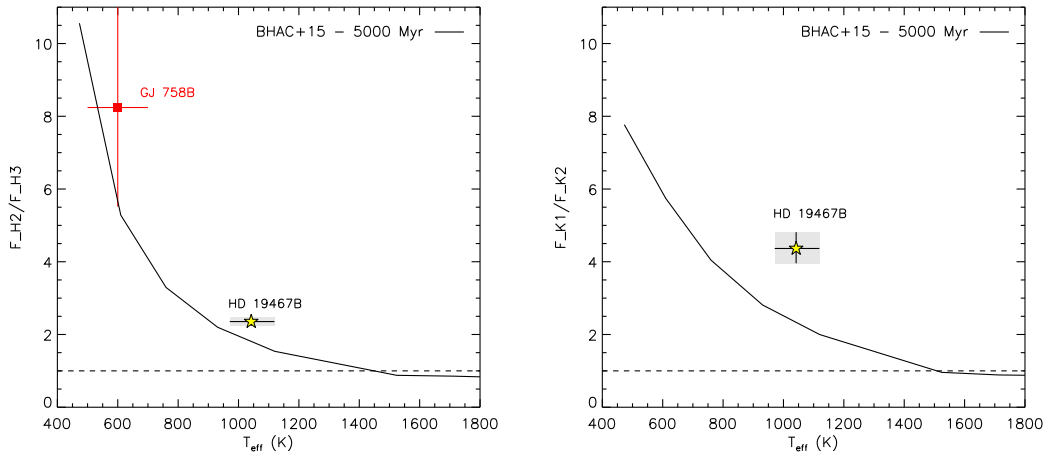

Fig. 18. Flux ratios outside and inside a methane absorption feature in the H band (*left*) and in the K_s band (*right*) as a function of the effective temperature of HD 19467B (star symbol) and GJ 758B (red square). The evolution predicted by the model of Baraffe et al. (2015) for an age of 5 Gyr is also shown (solid curve).

when including this effect. The main differences between the cloudless models of Saumon & Marley (2008) and the models of Burrows et al. (1997) are the use in the latter model of a lower value for the helium abundance (0.25 vs. 0.28 dex; the protosolar value is 0.2741 ± 0.0120, Lodders 2003) and a less opaque atmosphere. Both a lower helium abundance and a less opaque atmosphere result in lower luminosities.

Figure 17 compares the results from our atmospheric fits to the predictions of the four evolutionary models tested above in the effective temperature vs. surface gravity plane. We show model relations between these two parameters for several ages and companion masses. Only the atmospheric parameters derived from the petitCODE patchy fit are consistent with an object of the age of HD 19467B, when assuming the models COND and of Saumon & Marley (2008). For the models of Burrows et al. (1997), the predicted ages are too young, because for given age and $T_{\rm eff}$ the surface gravities predicted by this model are higher than those by the other models. The Exo-REM and Morley 2012 fits suggest too young ages and too low masses, whereas the petitCODE cloudy and clear fits suggest ages which are too young and too old, respectively. However, the temperature and surface gravity derived from the petitCODE patchy fit indicate a mass range slightly smaller (~57–66 M_J) than the mass range suggested by the orbital fit.

Finally, we compare in Fig. 18 the measured CH_4 flux ratios in the IRDIS narrow-band filters and the estimated effective temperature to the expectations from the model of Baraffe et al. (2015). We selected the model curve for an age of 5 Gyr, but we checked that the model curve for an age of 10 Gyr is very similar for the temperature range of HD 19467B. We computed flux ratios $F_{H2}/F_{H3} = 2.36^{+0.13}_{-0.12}$ and $F_{K1}/F_{K2} = 4.37^{+0.45}_{-0.41}$. The CH_4 flux ratio in the K_s band is ~1.9 times larger than the CH_4 flux ratio in the H band. The measured CH_4 flux ratio in the H band is close to the predictions given the effective temperature of HD 19467B estimated in our spectral analysis (Sect. 5.2), whereas the measured CH_4 flux ratio in the K_s band is larger than predicted.

The underpredicted bolometric luminosity by ~0.5 dex of evolutionary models with respect to the measured bolometric luminosity found in Wood et al. (2019) is due to a combination of slightly older age, brighter bolometric luminosity, and smaller dynamical mass estimated from the RV acceleration compared to our results.

7. Conclusions

We have presented VLT/SPHERE and VLT/NaCo observations of the benchmark T-type brown dwarf HD 19467B to further characterize its orbital and spectral properties. We have also refined the properties of the host star using archival data from ASAS, HARPS, and UVES. Our direct rotation period measurement indicates a gyrochronological age of 5.6 ± 0.8 Gyr, which is older than the range of 3.1–5.3 Gyr derived in Crepp et al. (2014) from an indirect rotation period estimate from chromospheric activity indicators. Our isochronal analysis suggests an older age of 9.3 ± 1.6 Gyr. The chemical abundances and kinematics of the star suggest an age younger than 10 Gyr and a possible membership to the thin disk population, which would set an upper age limit of ~8 Gyr. Considering potential biases in the gyrochronological and isochronal methods at low metallicities and/or ages older than the Sun, we estimated an age of $8.0^{+2.0}_{-1.0}$ Gyr. By fitting the SPHERE and NaCo data, archival RV data from HARPS and HIRES, literature imaging measurements from Keck/NIRC2, and HIPPARCOS-*Gaia* data, we derived constraints on the orbital parameters of HD 19467B and a dynamical mass of 65–86 M_J. We have further constrained the latter to 65–77 M_J using a theoretical limit on the hydrogen-burning mass limit. Our new photometric data extend the SED of the companion to the K and L' bands and confirm that the companion has a cool atmosphere. The spectrophotometric data of the companion are best fitted with model spectra of atmospheres with no clouds or very thin clouds for temperatures of 971–1118 K and high surface gravities of 5.25–5.42 dex. Finally, we have found that the measured bolometric luminosity and dynamical mass of HD 19467B are better reproduced by the evolutionary models of Burrows et al. (1997), whereas the models of Baraffe et al. (2003) and the models of Saumon & Marley (2008) tend to underestimate the cooling of the companion.

Further precise monitoring of the companion with both HARPS and high-contrast imaging in the coming years will be critical to measure at high significance an orbital curvature and place more robust upper limits on its dynamical mass. Spectral measurements at higher resolutions and/or at longer wavelengths will help to better constrain its atmospheric properties and chemical abundances. Finally, a more precise age estimate from asteroseismology will improve the comparison of the companion properties to model predictions and help to better distinguish them.

Acknowledgements. We thank an anonymous referee for a constructive report that helped to improve the manuscript. The authors thank the ESO Paranal Staff for support in conducting the observations and Eric Lagadec and Nadège Meunier (SPHERE Data Centre) for their help with the data reduction. We thank Justin Crepp for sending us the P1640 spectrum of HD 19467B during the revision of the manuscript for cross-checks. We thank Hans-Walter Rix for discussions regarding the use of stellar abundances for age determination. This work has made use of recipes from the IDL libraries: IDL Astronomy Users's Library (Landsman 1993), Coyote (http://www.idlcoyote.com/index.html), EXOFAST (Eastman et al. 2013), JBIU (http://www.simulated-galaxies.ua.edu/jbiu/), and the s3drs package (http://www.heliodocs.com/xdoc/index.html). It has also made use of the Python packages: NumPy (Oliphant 2006), emcee (Foreman-Mackey et al. 2013), corner (Foreman-Mackey 2016), Matplotlib (Hunter 2007), Astropy (Astropy Collaboration 2013, 2018), and dateutil (http://dateutil.readthedocs.io/). We acknowledge financial support from the Programme National de Planétologie (PNP) and the Programme National de Physique Stellaire (PNPS) of CNRS-INSU. This work has also been supported by a grant from the French Labex OSUG@2020 (Investissements d'avenir – ANR10 LABX56). The project is supported by CNRS, by the Agence Nationale de la Recherche (ANR-14-CE33-0018). This work has made use of the SPHERE Data Centre, jointly operated by OSUG/IPAG (Grenoble), PYTHEAS/LAM/CeSAM (Marseille), OCA/Lagrange (Nice), Observatoire de Paris/LESIA (Paris), and Observatoire de Lyon, also supported by a grant from Labex OSUG@2020 (Investissements d'avenir - ANR10 LABX56). T.H. acknowledges support from the European Research Council under the Horizon 2020 Framework Program via the ERC Advanced Grant Origins 83 24 28. This publication has made use of VOSA, developed under the Spanish Virtual Observatory project supported by the Spanish MINECO through grant AyA2017-84089. VOSA has been partially updated by using funding from the European Union's Horizon 2020 Research and Innovation Programme, under Grant Agreement n° 776403 (EXOPLANETS-A). This research has made use of the SIMBAD database and the VizieR Catalogue access tool, both operated at the CDS, Strasbourg, France. The original descriptions of the SIMBAD and VizieR services were published in Wenger et al. (2000) and Ochsenbein et al. (2000). This research has made use of NASA's Astrophysics Data System Bibliographic Services. SPHERE is an instrument designed and built by a consortium consisting of IPAG (Grenoble, France), MPIA (Heidelberg, Germany), LAM (Marseille, France), LESIA (Paris, France), Laboratoire Lagrange (Nice, France), INAF – Osservatorio di Padova (Italy), Observatoire de Genève (Switzerland), ETH Zurich (Switzerland), NOVA (Netherlands), ONERA (France), and ASTRON (Netherlands), in collaboration with ESO. SPHERE was funded by ESO, with additional contributions from CNRS (France), MPIA (Germany), INAF (Italy), FINES (Switzerland), and NOVA (Netherlands). SPHERE also received funding from the European Commission Sixth and Seventh Framework Programs as part of the Optical Infrared Coordination Network for Astronomy (OPTICON) under grant number RII3-Ct-2004-001566 for FP6 (2004–2008), grant number 226604 for FP7 (2009–2012), and grant number 312430 for FP7 (2013–2016).

References

Allard, F., Homeier, D., Freytag, B., & Sharp, C. M. 2012, EAS Pub. Ser., 57, 3
Amard, L., & Matt, S. P. 2020, ApJ, 889, 108
Asplund, M., Grevesse, N., Sauval, A. J., & Scott, P. 2009, ARA&A, 47, 481
Astropy Collaboration (Robitaille, T. P., et al.) 2013, A&A, 558, A33
Astropy Collaboration (Price-Whelan, A. M., et al.) 2018, AJ, 156, 123
Bailey, V., Meshkat, T., Reiter, M., et al. 2014, ApJ, 780, L4
Baraffe, I., Chabrier, G., Barman, T. S., Allard, F., & Hauschildt, P. H. 2003, A&A, 402, 701
Baraffe, I., Homeier, D., Allard, F., & Chabrier, G. 2015, A&A, 577, A42
Baudino, J. L., Bézard, B., Boccaletti, A., et al. 2015, A&A, 582, A83
Baudino, J.-L., Mollière, P., Venot, O., et al. 2017, ApJ, 850, 150
Bayo, A., Rodrigo, C., Barrado Y Navascués, D., et al. 2008, A&A, 492, 277
Beichman, C., Gelino, C. R., Kirkpatrick, J. D., et al. 2014, ApJ, 783, 68
Beuzit, J. L., Vigan, A., Mouillet, D., et al. 2019, A&A, 631, A155
Biller, B. A., Kasper, M., Close, L. M., Brandner, W., & Kellner, S. 2006, ApJ, 641, L141
Blunt, S., Nielsen, E. L., De Rosa, R. J., et al. 2017, AJ, 153, 229
Boccaletti, A., Sezestre, E., Lagrange, A.-M., et al. 2018, A&A, 614, A52
Bonnefoy, M., Chauvin, G., Lagrange, A.-M., et al. 2014, A&A, 562, A127
Bonnefoy, M., Perraut, K., Lagrange, A. M., et al. 2018, A&A, 618, A63
Boss, A. P. 1997, Science, 276, 1836
Bowler, B. P. 2016, PASP, 128, 102001
Bowler, B. P., Kraus, A. L., Bryan, M. L., et al. 2017, AJ, 154, 165
Bowler, B. P., Dupuy, T. J., Endl, M., et al. 2018, AJ, 155, 159
Bowler, B. P., Blunt, S. C., & Nielsen, E. L. 2020, AJ, 159, 63
Brandt, T. D. 2018, ApJS, 239, 31
Brandt, T. D. 2019, ApJS, 241, 39
Brandt, T. D., Dupuy, T. J., Bowler, B. P., et al. 2019a, AJ, submitted, [arXiv:1910.01652]
Brandt, T. D., Dupuy, T. J., & Bowler, B. P. 2019b, AJ, 158, 140
Bressan, A., Marigo, P., Girardi, L., et al. 2012, MNRAS, 427, 127
Burgasser, A. J. 2014, Astron. Soc. India Conf. Ser., 11, 7
Burningham, B., Pinfield, D. J., Leggett, S. K., et al. 2008, MNRAS, 391, 320
Burrows, A., Marley, M., Hubbard, W. B., et al. 1997, ApJ, 491, 856
Butler, R. P., Vogt, S. S., Laughlin, G., et al. 2017, AJ, 153, 208
Caffau, E., Ludwig, H. G., Steffen, M., Freytag, B., & Bonifacio, P. 2011, Sol. Phys., 268, 255
Calissendorff, P., & Janson, M. 2018, A&A, 615, A149
Cantalloube, F., Mouillet, D., Mugnier, L. M., et al. 2015, A&A, 582, A89
Carbillet, M., Bendjoya, P., Abe, L., et al. 2011, Exp. Astron., 30, 39
Castelli, F., & Kurucz, R. L. 2003, IAU Symp., 210, A20
Chabrier, G., & Baraffe, I. 1997, A&A, 327, 1039
Chabrier, G., Baraffe, I., Allard, F., & Hauschildt, P. 2000, ApJ, 542, 464
Charnay, B., Bézard, B., Baudino, J. L., et al. 2018, ApJ, 854, 172
Chauvin, G., Desidera, S., Lagrange, A.-M., et al. 2017a, in SF2A- 2017, eds. C. Reylé, P. Di Matteo, F. Herpin, E. Lagadec, A. Lançon, Z. Meliani, & F. Royer, 331
Chauvin, G., Desidera, S., Lagrange, A.-M., et al. 2017b, A&A, 605, L9
Cheetham, A., Bonnefoy, M., Desidera, S., et al. 2018, A&A, 615, A160
Cheetham, A. C., Samland, M., Brems, S. S., et al. 2019, A&A, 622, A80
Claudi, R. U., Turatto, M., Gratton, R. G., et al. 2008, SPIE Conf. Ser., 7014, 70143E
Crepp, J. R., Johnson, J. A., Howard, A. W., et al. 2014, ApJ, 781, 29
Crepp, J. R., Rice, E. L., Veicht, A., et al. 2015, ApJ, 798, L43
Cutri, R. M., Skrutskie, M. F., van Dyk, S., et al. 2003, VizieR Online Data Catalog: II/246
Cutri, R. M., et al. 2013, VizieR Online Data Catalog: II/328
da Silva, L., Girardi, L., Pasquini, L., et al. 2006, A&A, 458, 609
Dekker, H., D'Odorico, S., Kaufer, A., Delabre, B., & Kotzlowski, H. 2000, Proc. SPIEConf. Ser., 4008, 534
Delorme, P., Delfosse, X., Albert, L., et al. 2008, A&A, 482, 961
Delorme, P., Collier Cameron, A., Hebb, L., et al. 2011, MNRAS, 413, 2218
Delorme, P., Meunier, N., Albert, D., et al. 2017a, in SF2A- 2017, eds. C. Reylé, P. Di Matteo, F. Herpin, E. Lagadec, A. Lançon, Z. Meliani, & F. Royer, 347
Delorme, P., Schmidt, T., Bonnefoy, M., et al. 2017b, A&A, 608, A79
De Rosa, R. J., Patience, J., Ward-Duong, K., et al. 2014, MNRAS, 445, 3694
Desidera, S., Covino, E., Messina, S., et al. 2015, A&A, 573, A126
Dieterich, S. B., Weinberger, A. J., Boss, A. P., et al. 2018, ApJ, 865, 28
Dohlen, K., Langlois, M., Saisse, M., et al. 2008, SPIE Conf. Ser., 7014, 70143L
D'Orazi, V., Desidera, S., Gratton, R. G., et al. 2017, A&A, 598, A19
Ducourant, C., Teixeira, R., Galli, P. A. B., et al. 2014, A&A, 563, A121
Dupuy, T. J., & Kraus, A. L. 2013, Science, 341, 1492
Earl, D. J., & Deem, M. W. 2005, Phys. Chem. Che. Phys., 7, 3910
Eastman, J., Gaudi, B. S., & Agol, E. 2013, PASP, 125, 83
Faherty, J. K., Burgasser, A. J., Walter, F. M., et al. 2012, ApJ, 752, 56
Filippazzo, J. C., Rice, E. L., Faherty, J., et al. 2015, ApJ, 810, 158
Foreman-Mackey, D. 2016, J. Open Source Softw., 1, 24
Foreman-Mackey, D., Hogg, D. W., Lang, D., & Goodman, J. 2013, PASP, 125, 306
Frankel, N., Rix, H.-W., Ting, Y.-S., Ness, M., & Hogg, D. W. 2018, ApJ, 865, 96
Frankel, N., Sanders, J., Rix, H.-W., Ting, Y.-S., & Ness, M. 2019, ApJ, 884, 99
Fuhrmann, K., & Chini, R. 2019, MNRAS, 482, 471
Fuhrmann, K., Chini, R., Kaderhandt, L., & Chen, Z. 2017, MNRAS, 464, 2610
Gaia Collaboration (Prusti, T., et al.) 2016, A&A, 595, A1
Gaia Collaboration (Brown, A. G. A., et al.) 2018, A&A, 616, A1
Galicher, R., Boccaletti, A., Mesa, D., et al. 2018, A&A, 615, A92
Gauza, B., Béjar, V. J. S., Pérez-Garrido, A., et al. 2015, ApJ, 804, 96
Gizis, J. E., Allers, K. N., Liu, M. C., et al. 2015, ApJ, 799, 203
Goodman, J., & Weare, J. 2010, Commun. Appl. Math. Comput. Sci., 5, 65
Hayes, D. S. 1985, IAU Symp., 111, 225
Helou, G., & Walker, D. W. 1988, Infrared astronomical satellite (IRAS) catalogs and atlases. Volume 7: The small scale structure catalog, Vol. 7
Høg, E., Fabricius, C., Makarov, V. V., et al. 2000, A&A, 355, L27
Hunter, J. D. 2007, Comput. Sci. Eng., 9, 90
Janson, M., Carson, J., Thalmann, C., et al. 2011, ApJ, 728, 85
Janson, M., Brandt, T., Kuzuhara, M., et al. 2013, ApJ, 778, L4
Jensen-Clem, R., Millar-Blanchaer, M., Mawet, D., et al. 2016, ApJ, 820, 111
Kasper, M., Biller, B. A., Burrows, A., et al. 2007, A&A, 471, 655
Kasper, M., Burrows, A., & Brandner, W. 2009, ApJ, 695, 788
Kervella, P., Arenou, F., Mignard, F., & Thévenin, F. 2019, A&A, 623, A72
King, R. R., McCaughrean, M. J., Homeier, D., et al. 2010, A&A, 510, A99
Kirkpatrick, J. D., Reid, I. N., Liebert, J., et al. 2000, AJ, 120, 447
Kirkpatrick, J. D., Cushing, M. C., Gelino, C. R., et al. 2011, ApJS, 197, 19
Kirkpatrick, J. D., Gelino, C. R., Cushing, M. C., et al. 2012, ApJ, 753, 156

Kuzuhara, M., Tamura, M., Kudo, T., et al. 2013, ApJ, 774, 11
Lachapelle, F.-R., Lafrenière, D., Gagné, J., et al. 2015, ApJ, 802, 61
Lafrenière, D., Jayawardhana, R., & van Kerkwijk, M. H. 2010, ApJ, 719, 497
Lamm, M. H., Bailer-Jones, C. A. L., Mundt, R., Herbst, W., & Scholz, A. 2004, A&A, 417, 557
Landsman, W. B. 1993, ASP Conf. Ser., 52, 246
Langlois, M., Vigan, A., Moutou, C., et al. 2013, in Proceedings of the Third AO4ELT Conference, eds. S. Esposito, & L. Fini, 63
Leggett, S. K., Allard, F., Dahn, C., et al. 2000, ApJ, 535, 965
Lenzen, R., Hartung, M., Brandner, W., et al. 2003, SPIE Conf. Ser., 4841, 944
Lindegren, L., Hernández, J., Bombrun, A., et al. 2018, A&A, 616, A2
Liu, M. C., Fischer, D. A., Graham, J. R., et al. 2002, ApJ, 571, 519
Liu, M. C., Magnier, E. A., Deacon, N. R., et al. 2013, ApJ, 777, L20
Liu, M. C., Dupuy, T. J., & Allers, K. N. 2016, ApJ, 833, 96
Lo Curto, G., Pepe, F., Avila, G., et al. 2015, The Messenger, 162, 9
Lodders, K. 2003, ApJ, 591, 1220
Lomb, N. R. 1976, Ap&SS, 39, 447
Lucas, P. W., Tinney, C. G., Burningham, B., et al. 2010, MNRAS, 408, L56
Lucy, L. B., & Sweeney, M. A. 1971, AJ, 76, 544
Luhman, K. L., & Esplin, T. L. 2016, AJ, 152, 78
Mace, G. N., Kirkpatrick, J. D., Cushing, M. C., et al. 2013, ApJS, 205, 6
Macintosh, B., Graham, J. R., Barman, T., et al. 2015, Science, 350, 64
Maire, A.-L., Skemer, A. J., Hinz, P. M., et al. 2015, A&A, 576, A133
Maire, A.-L., Langlois, M., Dohlen, K., et al. 2016, SPIE Conf. Ser., 9908, 990834
Maire, A. L., Rodet, L., Cantalloube, F., et al. 2019, A&A, 624, A118
Maire, A. L., Baudino, J. L., Desidera, S., et al. 2020, A&A, 633, L2
Mamajek, E. E., & Hillenbrand, L. A. 2008, ApJ, 687, 1264
Marley, M. S., Fortney, J. J., Hubickyj, O., Bodenheimer, P., & Lissauer, J. 2007, ApJ, 655, 541
Marley, M. S., Saumon, D., Fortney, J. J., et al. 2017, AAS Meeting Abstracts, 230, 315.07
Marois, C., Lafrenière, D., Doyon, R., Macintosh, B., & Nadeau, D. 2006, ApJ, 641, 556
Marois, C., Correia, C., Galicher, R., et al. 2014, SPIE Conf. Ser., Vol. 9148, 91480U
Martinez, P., Dorrer, C., Aller Carpentier, E., et al. 2009, A&A, 495, 363
Mason, B. D., Hartkopf, W. I., Holdenried, E. R., & Rafferty, T. J. 2001, AJ, 121, 3224
Mawet, D., Milli, J., Wahhaj, Z., et al. 2014, ApJ, 792, 97
Mayor, M., Pepe, F., Queloz, D., et al. 2003, The Messenger, 114, 20
Mermilliod, J. C. 2006, VizieR Online Data Catalog: II/168
Mesa, D., Gratton, R., Zurlo, A., et al. 2015, A&A, 576, A121
Mesa, D., D'Orazi, V., Vigan, A., et al. 2020, MNRAS, 495, 4279
Messina, S., Desidera, S., Turatto, M., Lanzafame, A. C., & Guinan, E. F. 2010, A&A, 520, A15
Mollière, P., van Boekel, R., Dullemond, C., Henning, T., & Mordasini, C. 2015, ApJ, 813, 47
Mollière, P., van Boekel, R., Bouwman, J., et al. 2017, A&A, 600, A10
Morley, C. V., Fortney, J. J., Marley, M. S., et al. 2012, ApJ, 756, 172
Mountain, C. M., Leggett, S. K., Selby, M. J., Blackwell, D. E., & Petford, A. D. 1985, A&A, 151, 399
Mugnier, L. M., Cornia, A., Sauvage, J.-F., et al. 2009, J. Opt. Soc. Am. A, 26, 1326
Müller, A., Keppler, M., Henning, T., et al. 2018, A&A, 617, L2
Nakajima, T., Oppenheimer, B. R., Kulkarni, S. R., et al. 1995, Nature, 378, 463
Nissen, P. E. 2016, A&A, 593, A65
Ochsenbein, F., Bauer, P., & Marcout, J. 2000, A&AS, 143, 23
Oliphant, T. E. 2006, A Guide to NumPy (USA: Trelgol Publishing)
Patience, J., King, R. R., de Rosa, R. J., & Marois, C. 2010, A&A, 517, A76
Paunzen, E. 2015, A&A, 580, A23
Pavlov, A., Möller-Nilsson, O., Feldt, M., et al. 2008, SPIE Conf. Ser., Vol. 7019, 701939
Pinsonneault, M. H., Elsworth, Y. P., Tayar, J., et al. 2019, VizieR Online Data Catalog: J/ApJS/239/32
Pojmanski, G. 1997, Acta Astron., 47, 467
Prša, A., Harmanec, P., Torres, G., et al. 2016, AJ, 152, 41
Rajan, A., Rameau, J., De Rosa, R. J., et al. 2017, AJ, 154, 10
Rickman, E. L., Ségransan, D., Hagelberg, J., et al. 2020, A&A, 635, A203
Roberts, D. H., Lehar, J., & Dreher, J. W. 1987, AJ, 93, 968
Rohatgi, A. 2019, https://automeris.io/WebPlotDigitizer
Rousset, G., Lacombe, F., Puget, P., et al. 2003, SPIE Conf. Ser., 4839, 140
Samland, M., Mollière, P., Bonnefoy, M., et al. 2017, A&A, 603, A57
Saumon, D., & Marley, M. S. 2008, ApJ, 689, 1327
Scargle, J. D. 1982, ApJ, 263, 835
Schlieder, J. E., Skemer, A. J., Maire, A.-L., et al. 2016, ApJ, 818, 1
Schneider, A. C., Cushing, M. C., Kirkpatrick, J. D., et al. 2015, ApJ, 804, 92
Sneden, C. A. 1973, PhD thesis, The University of Texas at Austin, USA
Spina, L., Meléndez, J., Karakas, A. I., et al. 2018, MNRAS, 474, 2580
Stone, J. M., Skemer, A. J., Kratter, K. M., et al. 2016, ApJ, 818, L12
Tal-Or, L., Trifonov, T., Zucker, S., Mazeh, T., & Zechmeister, M. 2019, MNRAS, 484, L8
Thalmann, C., Carson, J., Janson, M., et al. 2009, ApJ, 707, L123
Tinney, C. G., Faherty, J. K., Kirkpatrick, J. D., et al. 2014, ApJ, 796, 39
Torres, G. 1999, PASP, 111, 169
Trifonov, T., Tal-Or, L., Zechmeister, M., et al. 2020, A&A, 636, A74
Ulrich, R. K. 1986, ApJ, 306, L37
van Leeuwen, F. 2007, A&A, 474, 653
van Saders, J. L., Ceillier, T., Metcalfe, T. S., et al. 2016, Nature, 529, 181
Vigan, A., Moutou, C., Langlois, M., et al. 2010, MNRAS, 407, 71
Vigan, A., Bonnefoy, M., Ginski, C., et al. 2016, A&A, 587, A55
Vogt, S. S., Allen, S. L., Bigelow, B. C., et al. 1994, Proc. SPIE, 2198, 362
Wahhaj, Z., Liu, M. C., Biller, B. A., et al. 2011, ApJ, 729, 139
Warren, S. J., Mortlock, D. J., Leggett, S. K., et al. 2007, MNRAS, 381, 1400
Wenger, M., Ochsenbein, F., Egret, D., et al. 2000, A&AS, 143, 9
Wood, C. M., Boyajian, T., von Braun, K., et al. 2019, ApJ, 873, 83
Wright, J. T. 2005, PASP, 117, 657
Wright, J. T., Marcy, G. W., Butler, R. P., & Vogt, S. S. 2004, ApJS, 152, 261
Zapatero Osorio, M. R., Béjar, V. J. S., Miles-Páez, P. A., et al. 2014, A&A, 568, A6

[1] STAR Institute, Université de Liège, Allée du Six Août 19c, 4000 Liège, Belgium
e-mail: almaire@uliege.be
[2] Max-Planck-Institut für Astronomie, Königstuhl 17, 69117 Heidelberg, Germany
[3] INAF – Osservatorio Astronomico di Padova, Vicolo dell'Osservatorio 5, 35122 Padova, Italy
[4] Department of Physics, University of Oxford, Oxford, UK
[5] LESIA, Observatoire de Paris, Université PSL, CNRS, Sorbonne Université, Univ. Paris Diderot, Sorbonne Paris Cité, 5 place Jules Janssen, 92195 Meudon, France
[6] INAF Catania Astrophysical Observatory, Via S. Sofia 78, 95123 Catania, Italy
[7] CNRS, IPAG, Univ. Grenoble Alpes, 38000 Grenoble, France
[8] INAF - Osservatorio Astronomico di Brera, Via E. Bianchi 46, 23807, Merate (Lc), Italy
[9] Institute for Astronomy, The University of Edinburgh, Royal Observatory, Blackford Hill View, Edinburgh, EH9 3HJ, UK
[10] Geneva Observatory, University of Geneva, Chemin des Maillettes 51, 1290 Versoix, Switzerland
[11] Unidad Mixta Internacional Franco-Chilena de Astronomía CNRS/INSU UMI 3386 and Departamento de Astronomía, Universidad de Chile, Casilla 36-D, Santiago, Chile
[12] CRAL, UMR 5574, CNRS, Université Lyon 1, ENS Lyon, 9 av. Charles André, 69561 Saint-Genis-Laval Cedex, France
[13] Aix-Marseille Université, CNRS, CNES, LAM, Marseille, France
[14] Department of Astronomy, University of Michigan, 1085 S. University Ave, Ann Arbor, MI 48109-1107, USA
[15] Dipartimento di Fisica e Astronomia "G. Galilei", Università di Padova, Via Marzolo, 8, 35121 Padova, Italy
[16] Instituto de Física y Astronomía, Facultad de Ciencias, Universidad de Valparaíso, Av. Gran Bretaña 1111, Playa Ancha, Valparaíso, Chile
[17] Núcleo Milenio Formación Planetaria - NPF, Universidad de Valparaíso, Av. Gran Bretaña 1111, Playa Ancha, Valparaíso, Chile
[18] Hamburger Sternwarte, Gojenbergsweg 112, 21029 Hamburg, Germany
[19] Núcleo de Astronomía, Facultad de Ingeniería y Ciencias, Universidad Diego Portales, Av. Ejercito 441, Santiago, Chile
[20] Escuela de Ingeniería Industrial, Facultad de Ingeniería y Ciencias, Universidad Diego Portales, Av. Ejercito 441, Santiago, Chile
[21] NOVA Optical Infrared Instrumentation Group, Oude Hoogeveensedijk 4, 7991 PD Dwingeloo, The Netherlands
[22] DOTA, ONERA, Université Paris Saclay, 91123 Palaiseau, France

Appendix A: Orbital fit on the imaging data

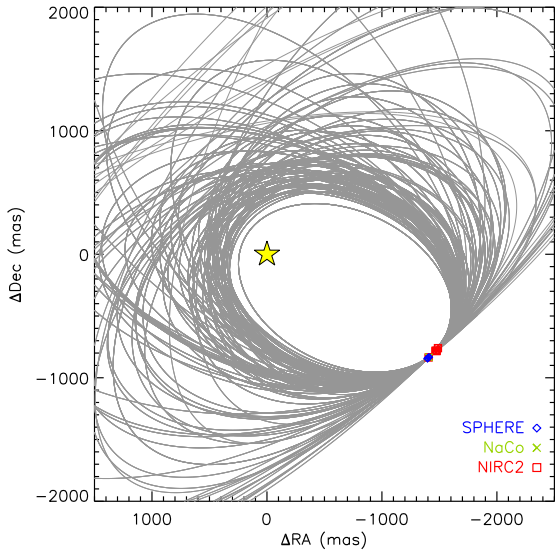

Fig. A.1. Sample of 100 orbits (gray curves) fitted on the imaging data (colored data points). The yellow star indicates the position of the star.

We fit the imaging data of HD 19467B using a custom implementation of the Bayesian rejection sampling approach Orbits For The Impatient (Blunt et al. 2017; Maire et al. 2019). We corrected the Keck and NaCo data for the systematics measured with respect to the SPHERE data in Sect. 4.3. We assumed uniform distributions in e, $\cos i$, ω, and T_0. Figure A.1 shows a sample of fitted orbits. Figure A.2 and Table A.1 show the derived orbital parameters based on the statistics of 27 374 fitted orbits. The longitude of the node and the argument of the periastron are restrained to the interval [0, 180) deg to account for the ambiguity on the longitude of the node inherent to the fitting of imaging data only.

Compared to the constraints derived in Bowler et al. (2020), our constraints agree given the uncertainties but are broader. We confirm that the orbital eccentricity of the companion is below 0.8. The most significant difference is for the longitude of the node. Our distribution for this parameter extends to values smaller than 60°, whereas no such values are found in Bowler et al. (2020).

Table A.1. Orbital parameters derived using the imaging data.

Parameter	Unit	Median ± 1σ	$\chi^2_{\rm min}$
P	yr	390^{+397}_{-154}	1324
a	au	52^{+31}_{-15}	119
e		$0.43^{+0.21}_{-0.23}$	0.20
i	°	127^{+17}_{-8}	112
Ω	°	88^{+44}_{-33}	120
ω	°	74^{+65}_{-36}	142
T_0	AD	2096^{+58}_{-231}	1674

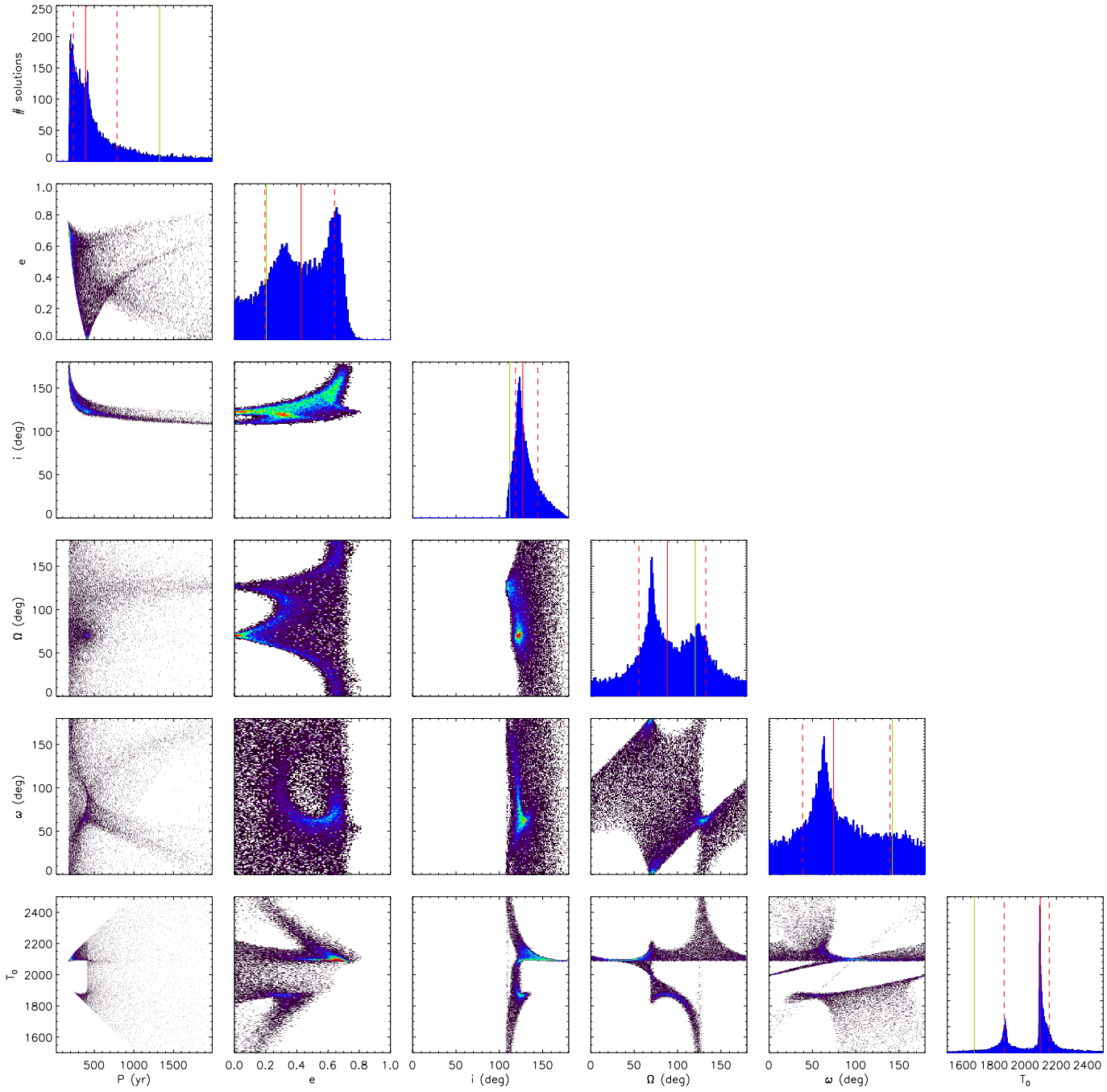

Fig. A.2. Posterior distributions of the orbital parameters obtained by fitting the imaging data. The diagrams displayed on the diagonal from *top left to lower right* represent the 1D histogram distributions for the individual elements. The off-diagonal diagrams show the correlations between pairs of orbital elements. The linear color-scale in the correlation plots accounts for the relative local density of orbital solutions. In the histograms, the green solid line indicates the best χ^2 fitted solution, the red solid line shows the 50% percentile value, and the red dashed lines represent the interval at 68%.

Appendix B: Orbital fit on the imaging and RV data

We fit the imaging and RV data of HD 19467B using a similar MCMC approach to Sect. 4.3. We sampled the parameter space of our 17-parameter model assuming 20 temperatures for the chains and 100 walkers. The first 8 parameters are the same as for the imaging-RV-astrometry fit in Sect. 4.3. We assumed similar priors. The next two parameters are the parallax and total mass of the system. We used the same prior on the parallax as in Sect. 4.3. We drew the system mass around a guess value of 1.015 $M_\odot$ considering a host star mass of 0.95 $M_\odot$ (Sect. 2) and a companion mass of 0.065 $M_\odot$ and assuming a Gaussian distribution with a half width at half maximum of 0.025 $M_\odot$. We included the prior information on the host star mass (0.95 ± 0.02 $M_\odot$) in the likelihood function instead of the system mass (by computing the difference between the fitted system mass and the companion mass derived from the binary mass function using the fitted orbital parameters). The remaining parameters and the associated priors are the same as in the imaging-RV fit.

Table B.1. Orbital parameters and dynamical mass of HD 19467B from the imaging-RV fit.

Parameter	Unit	Median ± 1σ	Best fit
Fitted parameters			
a	$''$	1652^{+516}_{-354}	1376
$\sqrt{e}\cos\omega$		-0.32 ± 0.06	−0.19
$\sqrt{e}\sin\omega$		$-0.69^{+0.11}_{-0.08}$	−0.75
i	°	130^{+12}_{-9}	140
Ω	°	135 ± 5	145
T_0	BJD	$2\,510\,135^{+25480}_{-15\,949}$	2 500 799
κ_A	m s^{-1}	263^{+69}_{-51}	210
π	mas	31.23 ± 0.12	31.05
System mass $M_{\rm tot}$	$M_\odot$	$1.024^{+0.030}_{-0.026}$	1.046
$\mathrm{ZP_{HARPS}}$	m s^{-1}	12.8 ± 0.7	12.8
$\mathrm{ZP_{HIRES}}$	m s^{-1}	-4.0 ± 0.9	−3.7
$\sigma_{\rm HARPS}$	m s^{-1}	$1.49^{+0.18}_{-0.15}$	1.39
$\sigma_{\rm HIRES}$	m s^{-1}	$3.9^{+0.6}_{-0.5}$	3.5
Sep. scaling $f\rho_{\rm NIRC2}$		$0.9955^{+0.0034}_{-0.0035}$	1.0023
PA offset $\Delta\mathrm{PA_{NIRC2}}$	°	$0.22^{+0.35}_{-0.34}$	0.16
PA offset $\Delta\mathrm{PA_{NaCo}}$	°	$-0.73^{+0.54}_{-0.55}$	−0.90
Computed parameters			
M_1	$M_\odot$	0.95 ± 0.02	0.99
M_2	M_J	74^{+23}_{-9}	63
M_2/M_1		$0.074^{+0.023}_{-0.010}$	0.061
P	yr	381^{+187}_{-114}	288
a	au	52^{+16}_{-11}	43
e		$0.58^{+0.11}_{-0.13}$	0.60
ω	°	65^{+6}_{-7}	76

We ran the MCMC analysis for 125 000 iterations and verified the convergence of the chains with the integrated autocorrelation time. Figure B.1 shows the posteriors on the parameters obtained after thinning the chains by a factor 100 and discarding the first 75% of the chains as the burn-in phase. Table B.1 gives the median values with 1σ uncertainties and the best-fit values. Figure B.2 shows a sample of fitted orbits.

Compared to a fit on the imaging data only (Appendix A), we note significant improvements on the derived parameters, especially the longitude of the ascending node, argument of the periastron, and eccentricity. For the eccentricity, values smaller than ∼0.19 are excluded, whereas for the imaging fit circular orbits are possible. The longitude of the ascending node and the time at the periastron do not show bimodal distributions. The longitude of the ascending node is restrained to values of 130–140° at 68%. The argument of the periastron is also better constrained to values of 58–71° at 68%. We also note correlations between parameters, with longer periods associated with smaller eccentricities, lower inclinations with respect to the line of sight, and larger RV semi-amplitudes.

Figure B.3 shows the posterior distributions for the masses of HD 19467 A and B as well as for the RV offsets and jitters. The mass posterior for HD 19467B exhibits a tail toward unphysically large masses beyond the hydrogen-burning mass limit, because the current data do not show a clear curvature.

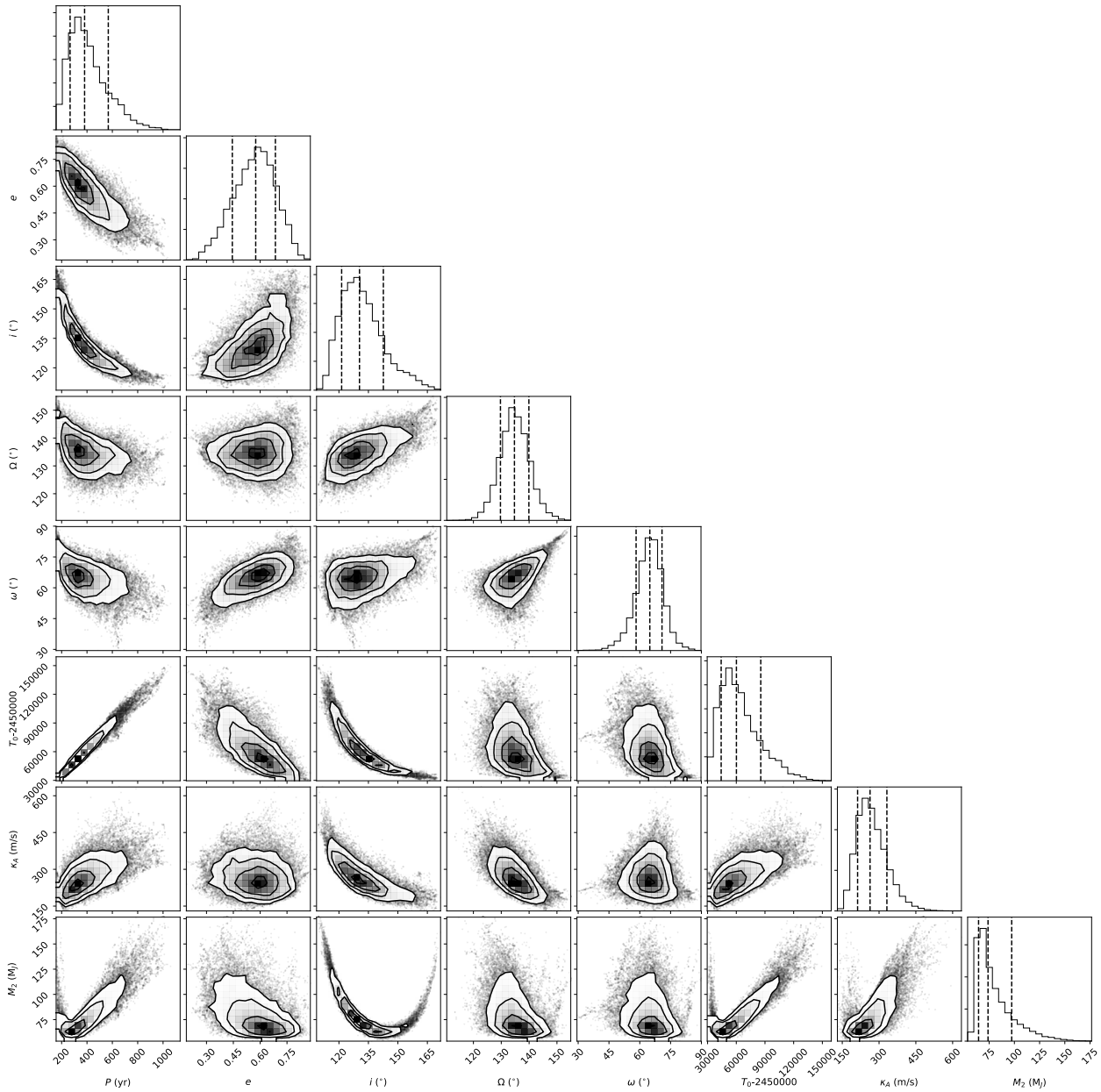

Fig. B.1. MCMC samples from the posteriors of the orbital parameters and of the mass of HD 19467B from the imaging-RV fit. See also Fig. 7.

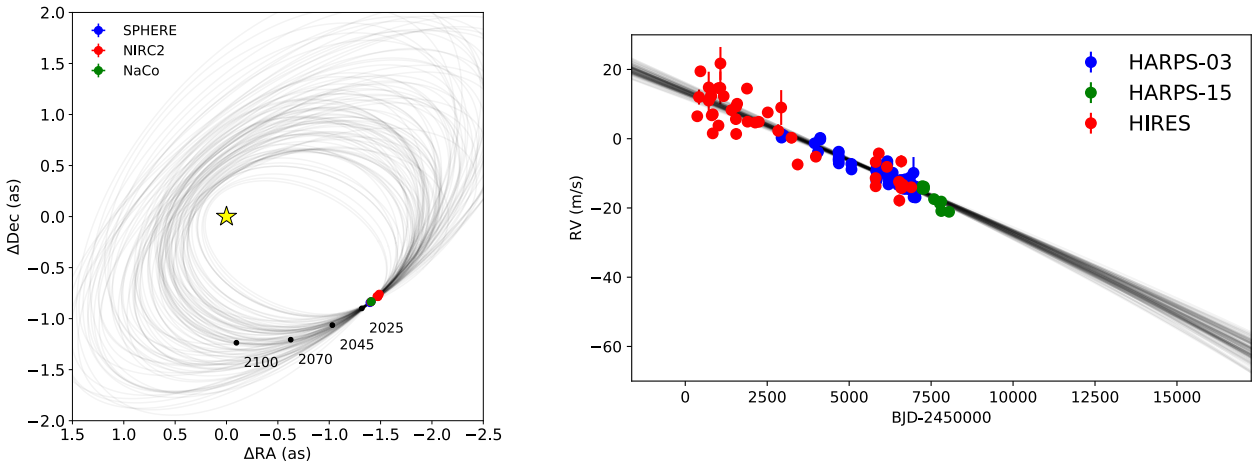

Fig. B.2. Sample of 100 model orbits (gray curves) fitted on the HD 19467B data points (colors) from imaging (*left*) and RV (*right*). In the left panel, the yellow star marks the position of the star and the black dots show the median predicted position for a few epochs in the future.

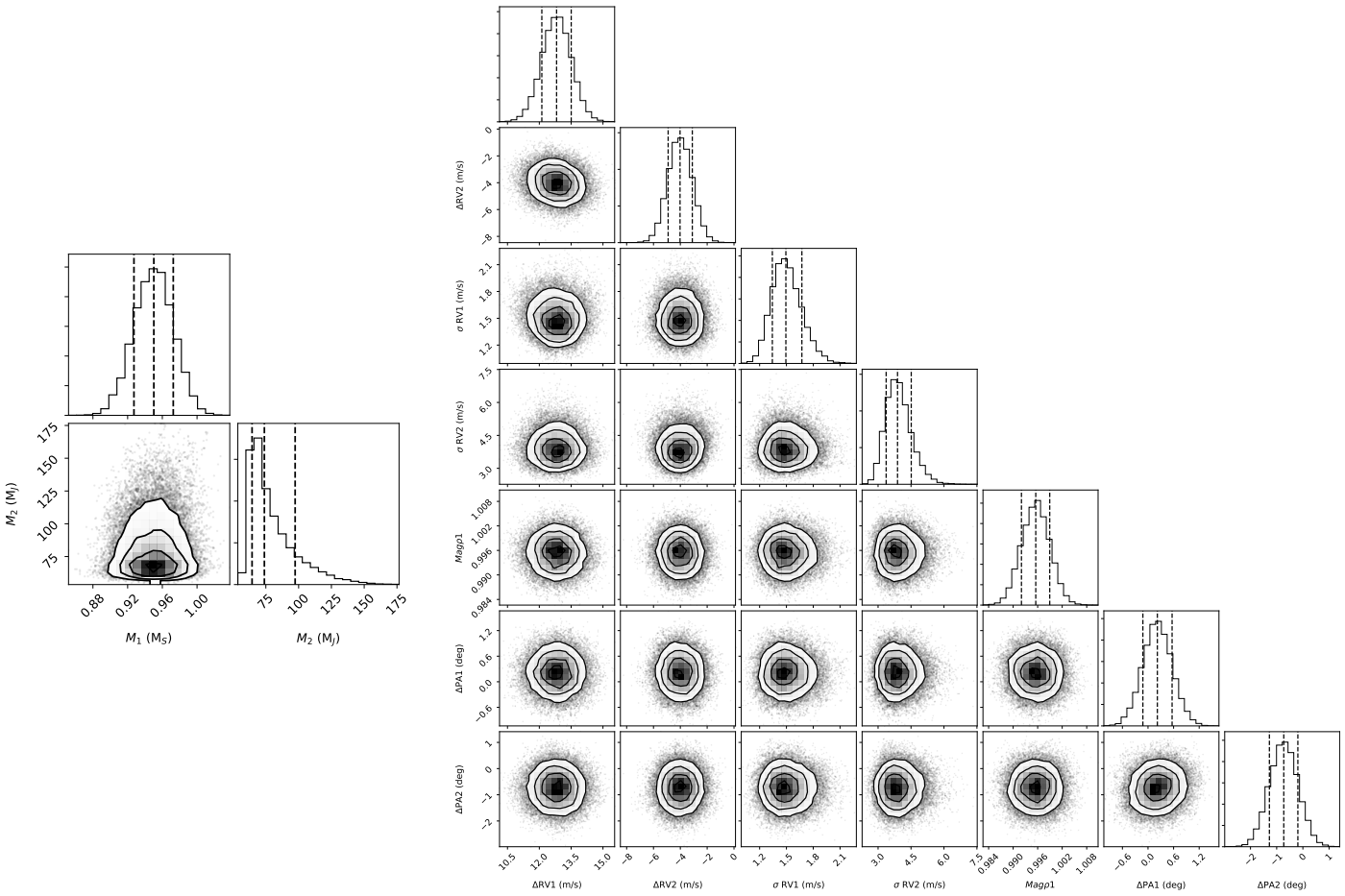

Fig. B.3. Same as in Fig. B.1, but for the masses of HD 19467 A and B (*left*) and for the RV offsets and jitters (1: HARPS, 2: HIRES) and the imaging offsets (1: Keck, 2: NaCo) (*right*).

Appendix C: Construction of the color-magnitude diagrams using narrow-band photometry

To build the diagrams shown in the top row of Fig. 9, we used spectra of M, L, and T dwarfs from the SpeX-Prism library (Burgasser 2014) and from Leggett et al. (2000) and Schneider et al. (2015) to generate synthetic photometry in the SPHERE filter passbands. The zero points were computed using a flux-calibrated spectrum of Vega (Hayes 1985; Mountain et al. 1985). We also considered the spectra of young and/or dusty free-floating objects from Liu et al. (2013), Mace et al. (2013), Gizis et al. (2015), and of young companions (Wahhaj et al. 2011; Gauza et al. 2015; Stone et al. 2016; De Rosa et al. 2014; Lachapelle et al. 2015; Bailey et al. 2014; Rajan et al. 2017; Bonnefoy et al. 2014, 2018; Patience et al. 2010; Lafrenière et al. 2010; Chauvin et al. 2017b; Delorme et al. 2017b; Cheetham et al. 2018). The colors and absolute fluxes of the benchmark companions and isolated T-type objects were generated from the distance and spectra of those objects in Appendix B in Bonnefoy et al. (2018). To conclude, we used the spectra of Y dwarfs published in Schneider et al. (2015), Warren et al. (2007), Delorme et al. (2008), Burningham et al. (2008), Lucas et al. (2010), Kirkpatrick et al. (2012), and Mace et al. (2013) to extend the diagrams in the late-T and early Y-dwarf domain. We used the distances of the field dwarfs reported in Kirkpatrick et al. (2000), Faherty et al. (2012), Dupuy & Kraus (2013), Tinney et al. (2014), Beichman et al. (2014), and Luhman & Esplin (2016). We considered those reported in Kirkpatrick et al. (2011), Faherty et al. (2012), Zapatero Osorio et al. (2014), and Liu et al. (2016) for the dusty dwarfs. The companion distances were taken from van Leeuwen (2007) and Ducourant et al. (2014).